Journal of Ecological Engineering, 2026, 27(1), 457–473 https://doi.org/10.12911/22998993/210422 ISSN 2299–8993, License CC-BY 4.0

Received: 2025.08.04 Accepted: 2025.10.08 Published: 2025.11.25

Satellite-based estimation and ground validation of air pollutants in a cement industry area in Indonesia

Putri Humaira Salsabila¹, Sumarni Hamid Aly^{1*}, Muralia Hustim¹, Nurul Masyiah Rani Harusi¹, Andi Azizah Nurul Dinanti¹, Hengky Pala'langan¹

- ¹ Department of Environmental Engineering, Universitas Hasanuddin, Malino Str. km 6, Gowa, South Sulawesi, 92171, Indonesia
- * Corresponding author's e-mail: marni hamidaly@yahoo.com

ABSTRACT

This study aimed to estimate the concentrations of air pollutants PM_{10} , NO_2 , SO_2 , and CO using Landsat 8 satellite imagery, validated with ground-based measurements at 41 monitoring points in the cement industry area of Pangkep Regency, South Sulawesi, Indonesia, and to evaluate air quality using ISPU indices. The methodology included radiometric and atmospheric correction of satellite imagery, extraction of spectral bands and land surface temperature, application of calibrated regression algorithms, comparison with ground-based measurements, as well as conversion of both satellite-derived and ground-based concentrations into ISPU indices to provide a comprehensive air quality assessment. The satellite-based estimations indicated PM_{10} concentrations of 4.55–4.56 μ g/m³, NO_2 of 23.59–72.15 μ g/m³, SO_2 of 75.79–231.79 μ g/m³, and CO of 83.3–83.6 μ g/m³. Validation results showed that the satellite-based estimates of NO_2 and SO_2 tended to be higher than ground-based measurements, whereas the PM_{10} and CO concentrations were lower than those measured in the field. Ground-based concentrations of the four pollutants, when converted into ISPU, ranging from Good to Moderate, while satellite-derived ISPU extended to the Unhealthy category. Despite these differences, the findings highlight the importance of integrating satellite imagery with ground-based observations to enhance air quality assessment, particularly in industrial regions with limited monitoring infrastructure.

Keywords: air pollution, satellite imagery, Landsat 8, ISPU, cement industry.

INTRODUCTION

Clean air is vital to ensuring human health and promoting overall well-being (Sannigrahi et al. 2021; South Australia EPA, 2023; United Nations, 2024). In general, polluted air is considered one of the primary contributors to various diseases, such as cardiovascular disorders, respiratory problems, and lung cancer. In addition, air pollution negatively impacts animals and harms plant ecosystems (Almetwally et al., 2020; Singh and Singh, 2022; Thongtip et al., 2022; John et al., 2025).

Air pollution is now broadly acknowledged as the leading environmental risk factor, with certain studies suggesting that poor air quality is associated with nearly 20% of deaths worldwide (Chen et al., 2024). Air pollution represents the foremost environmental exposure contributing to

global illness and death, placing fourth among all risk factors according to the 2019 Global Burden of Disease (GBD) study (Kuntic et al., 2023). Without substantial intervention, by 2060, ambient air pollution is expected to cause between 6 and 9 million deaths each year (Jasiński, 2024).

Increasing human activity, particularly in the industrial sector, has led to rising levels of air pollution (Siddiqua et al., 2022; Drahman et al., 2024; Nakhjiri and Kakroodi, 2024; Mohammed et al., 2024; Taufieq et al., 2024). Industrial operations significantly contribute to the emission of particulate matter (such as PM₁₀) and harmful gases (such as NO₂, SO₂, and CO) (Brontowiyono et al., 2022). Industrial processes involving fossil fuel combustion, raw material processing, and other operational activities release large volumes of pollutants into the atmosphere (Elawa and Farahat, 2022).

The cement industry, for example, is a major contributor to ambient air pollution. Approximately 5% of global carbon emissions originate from cement production. It is estimated that the production of one ton of cement clinker can emit up to 46.7 g of dust, 1.80 kg of NOx as NO₂, 0.504 kg of SO₂, among other pollutants (Al-Zboon et al., 2021). The cement sector holds significant importance in driving national development and fostering economic growth. It serves as a key material extensively utilized in construction and infrastructure development initiatives (Sudhakar and Reddy, 2023). It is the most common and extensively used binding material in the construction industry, found in roads, housing, embankments, bridges, commercial buildings, and overpasses. Therefore, the production of cement has significantly contributed to global economic progress, underpinning major infrastructure sectors worldwide, including construction, steel, petroleum, iron, and telecommunications (Etim et al., 2021).

The air pollution resulting from the cement industry poses a significant challenge, particularly in developing countries, such as Indonesia. The growing demand for cement in Indonesia reflects a substantial increase, with sales forecasted to rise by 4.9% from the preceding year to 73 million tons in 2019, aligning with the intensification of infrastructure development at the national level (Pambudi et al., 2020).

As one of the largest cement producers in Indonesia, monitoring air quality in cement industry areas is crucial to protect public health and the environment. However, the availability of air quality monitoring stations in several regions across Indonesia remains limited, making it difficult to obtain comprehensive air quality data. According to the data from IQAir (2024), there are only three air monitoring stations in South Sulawesi – two in Makassar City and one in Maros Regency.

In response to this limitation, remote sensing has emerged as a viable method for measuring or estimating air quality. Remote sensing technology based on satellites provides an efficient method for long-term air quality monitoring across different spatial and temporal scales. The advancement of satellite remote sensing has made satellite imagery a vital tool in observing urban ecological conditions, owing to its high spatial resolution, extensive coverage, and fast data acquisition (Wang et al., 2022).

Monitoring of air pollution using satellite imagery has been in practice since the 1970s, initiated with the deployment of instruments such as AVHRR and GOES. Today, satellites like Sentinel and Landsat are widely used for evaluating air quality (Ghasempour et al., 2021).

As a member of the Landsat series, Landsat 8 is frequently employed in air quality studies. It is equipped with two key instruments: the Operational Land Imager (OLI) and the Thermal Infrared Sensor (TIRS), which offer global land coverage on a seasonal basis. The satellite provides data at spatial resolutions of 30 meters (visible, NIR, SWIR), 100 meters (thermal), and 15 meters (panchromatic). The mission was developed collaboratively by NASA and the U.S. Geological Survey (USGS) (NASA, 2024).

Estimating air pollutant concentrations using Landsat 8 imagery offers the opportunity to map the spatial and temporal distribution of air pollution around cement industry areas. However, a comparison between the air quality data obtained from both satellite and ground-based platforms is necessary to assess the strengths and limitations of each in detecting and measuring pollutant concentrations. This comparison may also serve as a foundation for developing more effective satellite-based air quality monitoring methods, especially in the areas with limited air monitoring infrastructure. This analysis is expected to contribute meaningfully to the enhancement of air quality monitoring systems and efforts to mitigate the impacts of air pollution in Indonesia.

To evaluate and communicate the severity of air pollution, standardized air quality indices are widely used. Indonesia employs the Air Pollution Standard Index (ISPU), as defined in Government Regulation No. 22 of 2021, which categorizes air quality into five levels to inform the public about health risks. This index allows for spatial comparison of air quality across regions and serves as a critical tool for environmental management as well as policy-making. In the areas with limited monitoring stations, integrating satellite-based pollutant estimation with ISPU can enhance air quality surveillance and public health protection.

Unlike most previous studies, the novelty of this study lies in its dual approach: applying empirically validated algorithms to estimate pollutants using Landsat 8 imagery, and comparing these estimates against ground-based measurements to assess accuracy and reliability. Furthermore, by incorporating the Indonesian Air Pollution Standard

Index (ISPU), the study provides a framework for evaluating air quality that is both locally relevant and practically applicable. This approach offers new insights into the strengths and limitations of satellite remote sensing in capturing pollution dynamics in industrial regions where monitoring infrastructure remains scarce.

METHODOLOGY

Study area

The study was conducted in Pangkep Regency, South Sulawesi, Indonesia, focusing on one of the largest cement industry complexes in the country. This industrial area plays a vital role in national infrastructure development, but also represents a significant source of air pollution due to quarrying, clinker production, coal combustion, and cement milling activities. The region is geographically located in a coastal-to-hinterland transition zone, characterized by limestone hills and surrounding residential settlements.

The cement industry in Pangkep consists of multiple operational units, including clay quarries, limestone quarries, cement mills, coal stockpiles, and power plants. These facilities release various air pollutants, notably particulate matter (PM₁₀), nitrogen dioxide (NO₂), sulfur dioxide (SO₂), and carbon monoxide (CO), which can affect both the industrial workforce and nearby communities.

To capture the spatial variations in air quality, a total of 41 monitoring points were selected, covering both industrial zones and residential areas. The industrial monitoring points were located around major emission sources, such as quarries, cement mills, and power plants, while the residential points were distributed in nearby villages and along main roads. The spatial distribution of these points is shown in Figure 1, and their detailed locations are listed in Table 1.

Dataset and methods

This study employed a quantitative research design with a descriptive-comparative approach to evaluate air quality conditions around Cement Industry X in Pangkep Regency. The analysis considered PM₁₀, NO₂, SO₂, and CO as target pollutants, while the satellite spectral data were used as predictors for their estimation.

Dataset

Two primary datasets were utilized in this study. The first dataset consisted of Landsat 8

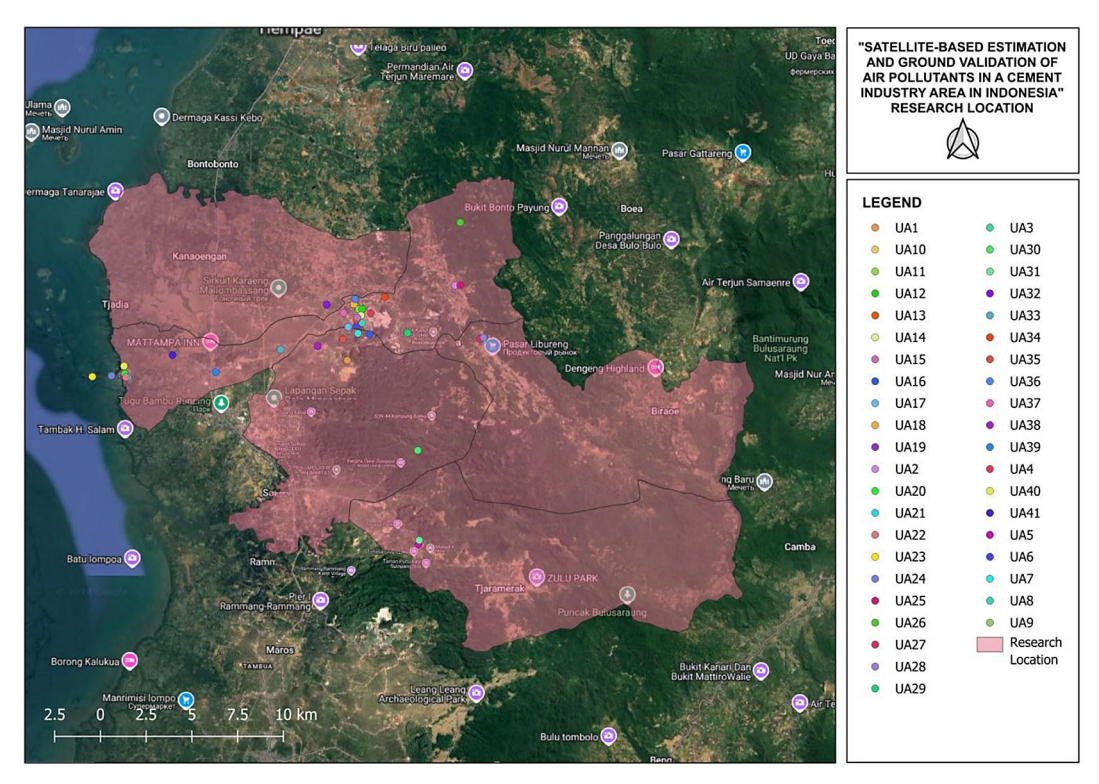


Figure 1. Research location

Table 1. Measurement points

Area	Measurement points	Code
	Bontoa Clay Quarry	UA1
	Tabo-Tabo Clay Quarry	UA2
	Bulutellue Clay Quarry	UA3
	Limestone Quarry	UA4
	Tonasa 1 Clay Quarry	UA5
	Packer Unit 5	UA6
	Cement Mill Unit 5	UA7
	Kiln Unit 5	UA8
	Packer Unit 2/3/4	UA9
	Cement Mill Unit 2/3	UA10
	Coal Mill Unit 2/3	UA11
Ou	Kiln Unit 2/3	UA12
Operational area	Coal Stock Pile Unit 2/3/4	UA13
	Kiln Unit 4	UA14
	Cement Mill Unit 4	UA15
	Coal Stockpile Unit 5	UA16
	Coal Stockpile Bontoa	UA17
	Batching Plant Biringere	UA18
	Biringkassi Coal Warehouse	UA19
	Biringkassi Cement Silo	UA20
	Biringkassi Power Plant 1	UA21
	Biringkassi Power Plant 2	UA22
	Central Special Wharf of Biringkassi	UA23
	Wharf II Biringkassi	UA24
	Road near Tabo-Tabo Clay Quarry	UA25
	Residential Area near Tabo-Tabo Quarry	UA26
	Residential Area near Bulutellue Quarry	UA27
	Road near Bulutellue Clay Quarry	UA28
	Mangilu Village	UA29
	Road near Tonasa 1 Clay Quarry	UA30
	Residential Area near Tonasa 1 Clay Quarry	UA31
	Taraweang Village	UA32
Residential area	In Front of Sapanang Village Office	UA33
	In Front of Kampung Sela Mosque	UA34
	In Front of Main Office	UA35
	Biringere Village Office	UA36
	In Front of Taqwa Mosque	UA37
	Tonasa–Bungoro Main Road (Bontoa)	UA38
	Bungoro Intersection	UA39
	In Front of Bujung Tangaya Elementary School (Bulu Cindea)	UA40
	Bowong Cindea Village	UA41

OLI and TIRS imagery obtained from the United States Geological Survey (USGS), which provides spectral information at 30 m (visible, NIR, SWIR), 100 m (thermal), and 15 m (panchromatic) spatial resolutions. Preprocessing steps included

radiometric correction, atmospheric correction, and raster clipping to match the Area of Interest (AOI). From these images, spectral bands (blue, green, red, SWIR-2) and Land Surface Temperature (LST) were extracted as inputs for pollutant

estimation. The second dataset involved ground-based measurements, consisting of ground-based measurements concentrations for PM₁₀, NO₂, SO₂, and CO obtained from 41 monitoring points distributed across both industrial and residential zones (Table 1). These field data were used as validation for the satellite-derived estimates.

Methods

The research workflow began with the preprocessing of Landsat 8 imagery, which included defining the Area of Interest (AOI), raster clipping, as well as applying radiometric and atmospheric corrections to ensure data accuracy. After preprocessing, input variables were extracted from the imagery, particularly the blue, green, red, and SWIR-2 spectral bands, as well as Land Surface Temperature (LST), all of which served as the basis for pollutant estimation. Pollutant concentrations were then estimated by applying empirical algorithms that had been validated in previous studies, with PM₁₀ calculated using the model proposed by Othman et al. (2010) (Equation 1), NO₂ and SO₂ estimated using the algorithms developed by Mahardianti et al. (2024) (Equations 2 and 3), and CO calculated according to the model of Somvanshi et al. (2019) (Equation 4).

$$PM_{10} = (396 \times \beta 2) + + (253 \times \beta 3) - (194 \times \beta 4)$$
 (1)

$$NO_2 = LST \times 1.875 \tag{2}$$

$$SO_2 = LST \times 6.0232 \tag{3}$$

$$CO = 83.659 + (-0.427 \times \beta 3) + + (0.22 \times \beta 4) + (-0.461 \times \beta 7)$$
 (4)

where: $\beta 2$ – blue band, $\beta 3$ – green band, $\beta 4$ – red band, $\beta 7$ – SWIR 2 band, LST – Land Surface Temperature

The estimated values obtained from these algorithms were validated against the ground-based measurements collected from the 41 monitoring points to assess the level of agreement and identify potential discrepancies. Following validation, the data were analyzed spatially to map the distribution of pollutants across the study area. To further interpret the health implications of the estimated pollutant concentrations, the ISPU, as defined in Indonesian Government Regulation No. 22 of 2021, was calculated. The index values were derived using the following formula (Equation 5):

$$I = \frac{I_{\text{high}} - I_{\text{tow}}}{C_{\text{high}} - C_{\text{low}}} \cdot (C - C_{\text{low}}) + I_{\text{low}}$$
(5)

where: I — ISPU value for pollutant concentration C, C — actual pollutant concentration, C_{high} , C_{low} — upper and lower concentration bounds for the ISPU category in which C falls, I_{high} , I_{low} — corresponding upper and lower ISPU values for C_{high} and C_{low}

RESULTS

This study aimed to address three main questions, namely whether Landsat 8 satellite imagery can be applied to estimate concentrations of PM₁₀, NO₂, SO₂, and CO in a cement industrial area, how these satellite-based estimations compare with ground-based measurements, and how the overall air quality can be categorized using ISPU. The following subsections present the results in line with these research questions.

Estimation of air pollutant concentrations based on satellite imagery

As a basis for further analysis, the estimated concentrations of air pollutants derived from Landsat 8 imagery are first presented. The estimations were obtained through empirically validated regression algorithms for PM₁₀, NO₂, SO₂, and CO, using spectral reflectance and land surface temperature (LST) as input variables. These results provide an initial overview of the pollutant levels in the study area and serve as a reference point for subsequent comparisons with field measurements and spatial visualization.

Table 2 shows the estimated concentrations of PM_{10} , NO_2 , SO_2 , and CO at 41 observation points representing both industrial and residential areas surrounding the cement production complex. The estimates indicate spatial variation, with higher pollutant concentrations generally observed near core industrial operations, such as quarry sites, cement mills, and coal-fired power plants. Specifically, the PM_{10} concentrations ranged between 4.55 and 4.56 $\mu g/m^3$, NO_2 between 23.59 and 72.15 $\mu g/m^3$, SO_2 between 75.79 and 231.79 $\mu g/m^3$, and CO around 83.3–83.6 $\mu g/m^3$. These values serve as the basis for further analysis, including comparison with field measurements and

Table 2. Estimation of air pollutant concentrations based on satellite imagery

Area	Measurement points	Code	Pollutant concentrations (µg/m³)			
Area	Measurement points	Code	PM ₁₀	NO ₂	SO ₂	СО
	Bontoa Clay Quarry	UA1	4.550	57.06	183.30	83.56
	Tabo-Tabo Clay Quarry	UA2	4.551	72.15	231.79	83.52
	Bulutellue Clay Quarry	UA3	4.551	65.84	211.50	83.52
	Limestone Quarry	UA4	4.557	23.59	75.79	83.26
	Tonasa 1 Clay Quarry	UA5	4.551	66.88	214.83	83.53
	Packer Unit 5	UA6	4.552	37.50	120.46	83.48
	Cement Mill Unit 5	UA7	4.552	39.82	127.93	83.48
	Kiln Unit 5	UA8	4.554	25.88	83.13	83.36
	Packer Unit 2/3/4	UA9	4.553	23.88	76.71	83.46
	Cement Mill Unit 2/3	UA10	4.552	32.09	103.10	83.47
	Coal Mill Unit 2/3	UA11	4.551	38.60	124.01	83.59
Operational area	Kiln Unit 2/3	UA12	4.554	25.46	81.78	83.35
Operational area	Coal Stock Pile Unit 2/3/4	UA13	4.552	38.07	122.28	83.53
	Kiln Unit 4	UA14	4.552	42.40	136.19	83.49
	Cement Mill Unit 4	UA15	4.552	40.21	129.16	83.51
	Coal Stockpile Unit 5	UA16	4.551	36.54	117.37	83.52
	Coal Stockpile Bontoa	UA17	4.552	33.09	106.30	83.52
	Batching Plant Biringere	UA18	4.551	42.73	137.25	83.57
	Biringkassi Coal Warehouse	UA19	4.550	61.98	199.09	83.54
	Biringkassi Cement Silo	UA20	4.551	63.32	203.40	83.57
	Biringkassi Power Plant 1	UA21	4.550	59.66	191.64	83.57
	Biringkassi Power Plant 2	UA22	4.550	60.22	193.45	83.54
	Central Special Wharf of Biringkassi	UA23	4.551	49.66	159.52	83.53
	Wharf II Biringkassi	UA24	4.551	51.81	166.43	83.55
	Road near Tabo-Tabo Clay Quarry	UA25	4.551	68.75	220.85	83.53
	Residential Area near Tabo-Tabo Quarry	UA26	4.550	51.42	165.17	83.60
	Residential Area near Bulutellue Quarry	UA27	4.550	64.29	206.51	83.56
	Road near Bulutellue Clay Quarry	UA28	4.551	64.49	207.17	83.54
	Mangilu Village	UA29	4.551	69.41	222.97	83.53
	Road near Tonasa 1 Clay Quarry	UA30	4.550	51.83	166.51	83.57
	Residential Area near Tonasa 1 Clay Quarry	UA31	4.550	66.33	213.09	83.55
	Taraweang Village	UA32	4.551	69.52	223.33	83.52
Residential area	In Front of Sapanang Village Office	UA33	4.551	69.49	223.23	83.55
	In Front of Kampung Sela Mosque	UA34	4.554	29.87	95.95	83.34
	In Front of Main Office	UA35	4.550	59.10	189.86	83.61
	Biringere Village Office	UA36	4.551	45.99	147.72	83.54
	In Front of Taqwa Mosque	UA37	4.550	58.80	188.90	83.60
	Tonasa–Bungoro Main Road (Bontoa)	UA38	4.551	69.34	222.74	83.53
	Bungoro Intersection	UA39	4.551	64.60	207.52	83.55
	In Front of Bujung Tangaya Elementary School (Bulu Cindea)	UA40	4.551	60.72	195.07	83.54
	Bowong Cindea Village	UA41	4.550	61.00	195.97	83.52

spatial distribution mapping through graphs and thematic maps in the subsequent sections.

Comparison of satellite imagery estimation with ground-based measurements

To assess the accuracy of the satellite-based estimates, the results were compared with ground-based measurements. Figures 2, 4, 6, and 8 present the comparison between the estimated and measured concentrations of PM₁₀, NO₂, SO₂, and CO, while Figures 3, 5, 7, and 9 illustrate their spatial distribution across the study area.

In Figures 2 and 3, it can be observed that based on satellite imagery estimation, the highest PM₁₀ concentration was found at UA4 (Limestone Quarry), and the lowest at UA35 (In Front of Main Office). However, based on the measurement data, the highest PM₁₀ concentration was found at UA7 (Cement Mill Unit 5), while the lowest at UA26 (Residential Area near Tabo-Tabo Quarry).

Figures 4 and 5 show that based on satellite imagery estimation, the highest NO₂ concentration was found at UA2 (Tabo-Tabo Clay Quarry), and the lowest at UA4 (Limestone Quarry).

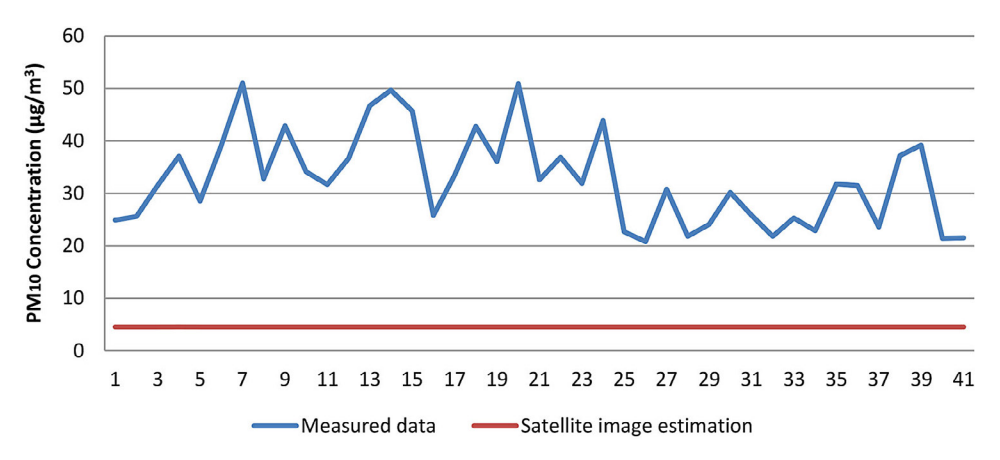


Figure 2. Comparison of PM_{10} concentrations

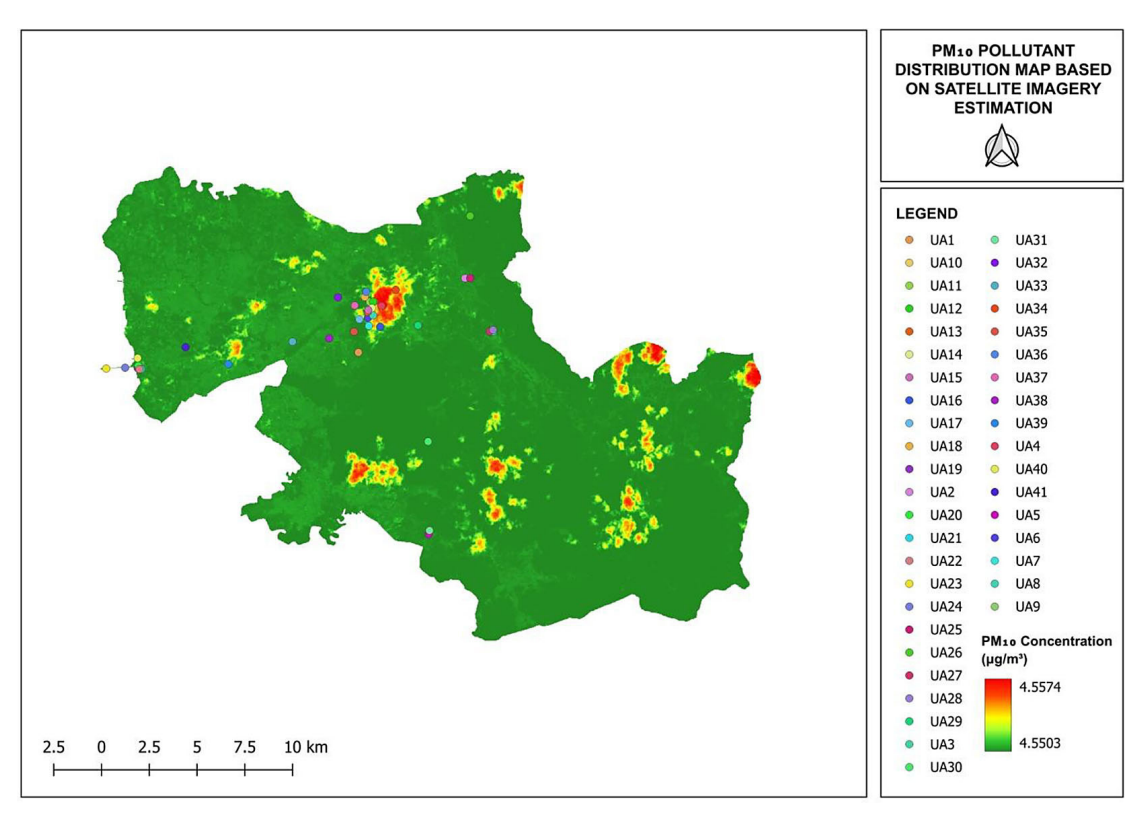


Figure 3. PM₁₀ pollutant distribution map based on satellite imagery estimation

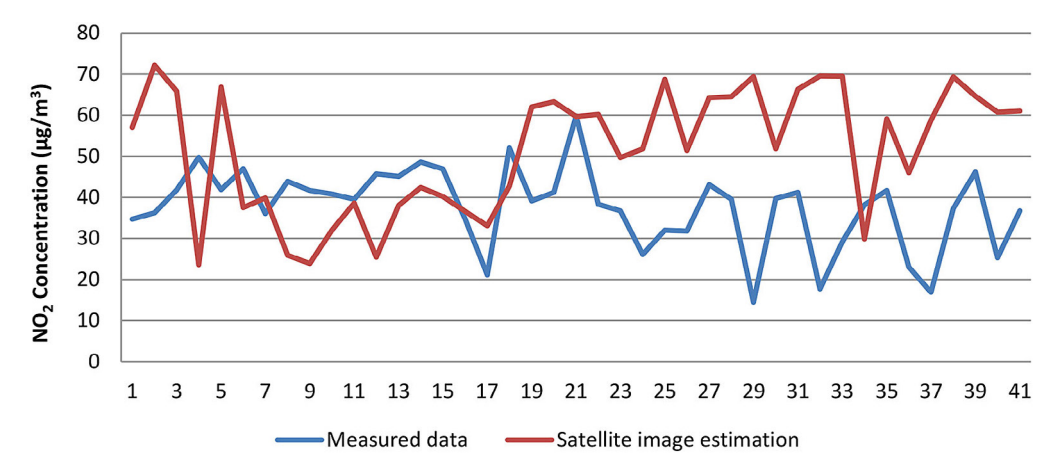


Figure 4. Comparison of NO, concentrations

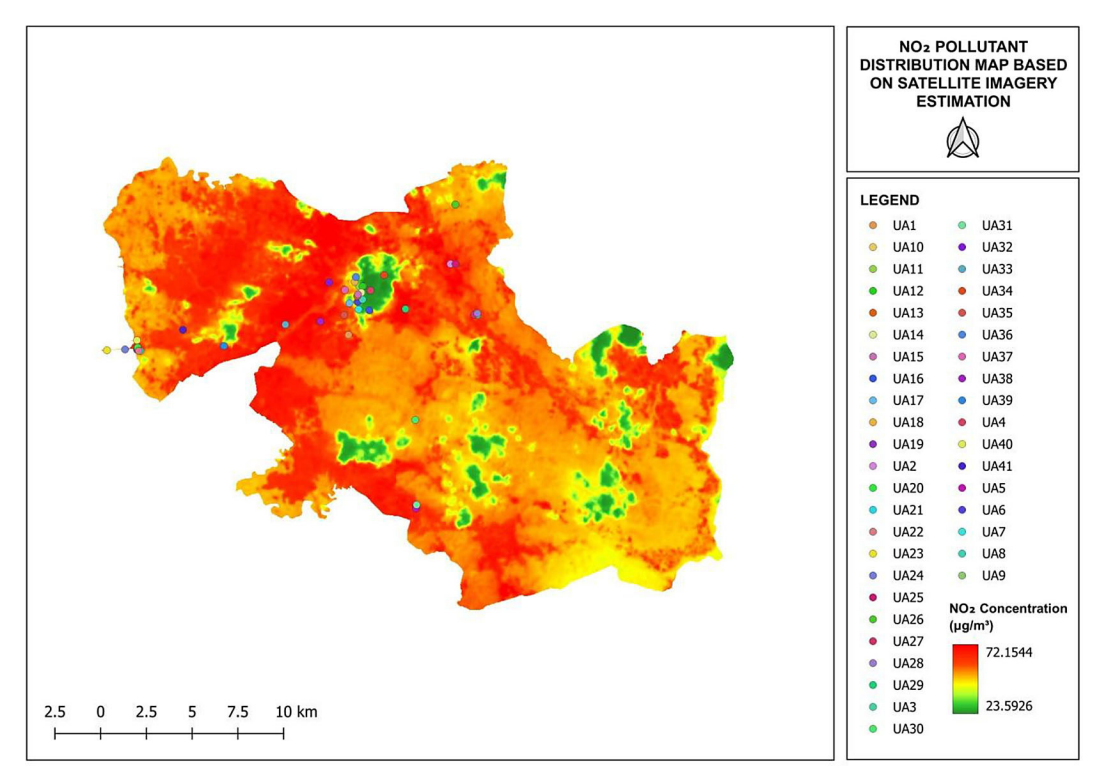


Figure 5. NO, pollutant distribution map based on satellite imagery estimation

Meanwhile, based on the measurement data, the highest NO₂ concentration was found at UA21 (Biringkassi Power Plant 1), and the lowest at UA29 (Mangilu Village).

In Figures 6 and 7, it can be seen that based on satellite imagery estimation, the highest SO₂ concentration was found at UA2 (Tabo-Tabo Clay Quarry), and the lowest at UA4 (Limestone Quarry). However, based on the measurement data, the highest SO₂ concentration was found at UA38 (Tonasa–Bungoro Main Road (Bontoa)), and the lowest at UA40 (In Front of Bujung Tangaya Elementary School (Bulu Cindea)).

Figures 8 and 9 show that based on satellite imagery estimation, the highest CO concentration was found at UA35 (In Front of Main Office), and the lowest at UA4 (Limestone Quarry). Meanwhile, based on the measurement data, the highest CO concentration was found at UA9 (Packer Unit 2/3/4), and the lowest at UA40 (In Front of Bujung Tangaya Elementary School (Bulu Cindea)).

Air pollution standard index

The estimated concentrations of pollutants were further translated into the air pollution standard index (ISPU) to provide a more interpretable

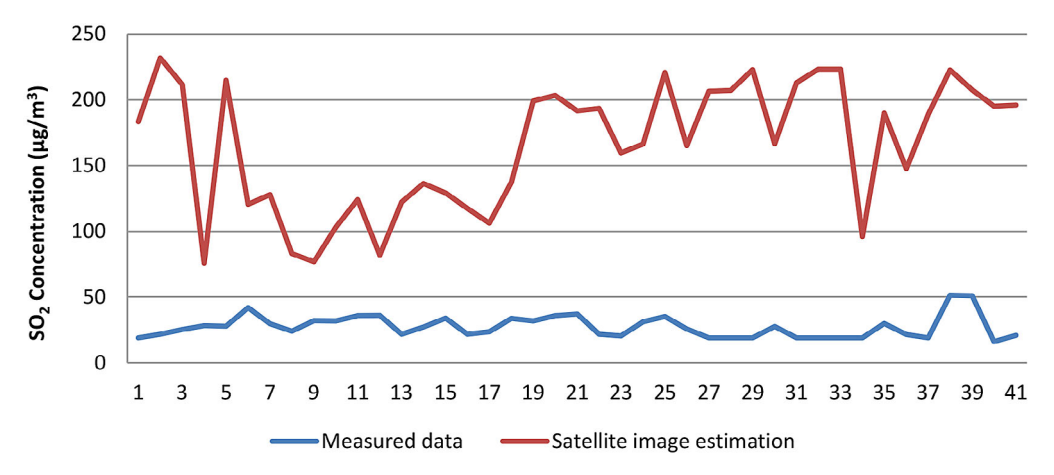


Figure 6. Comparison of the SO, concentrations

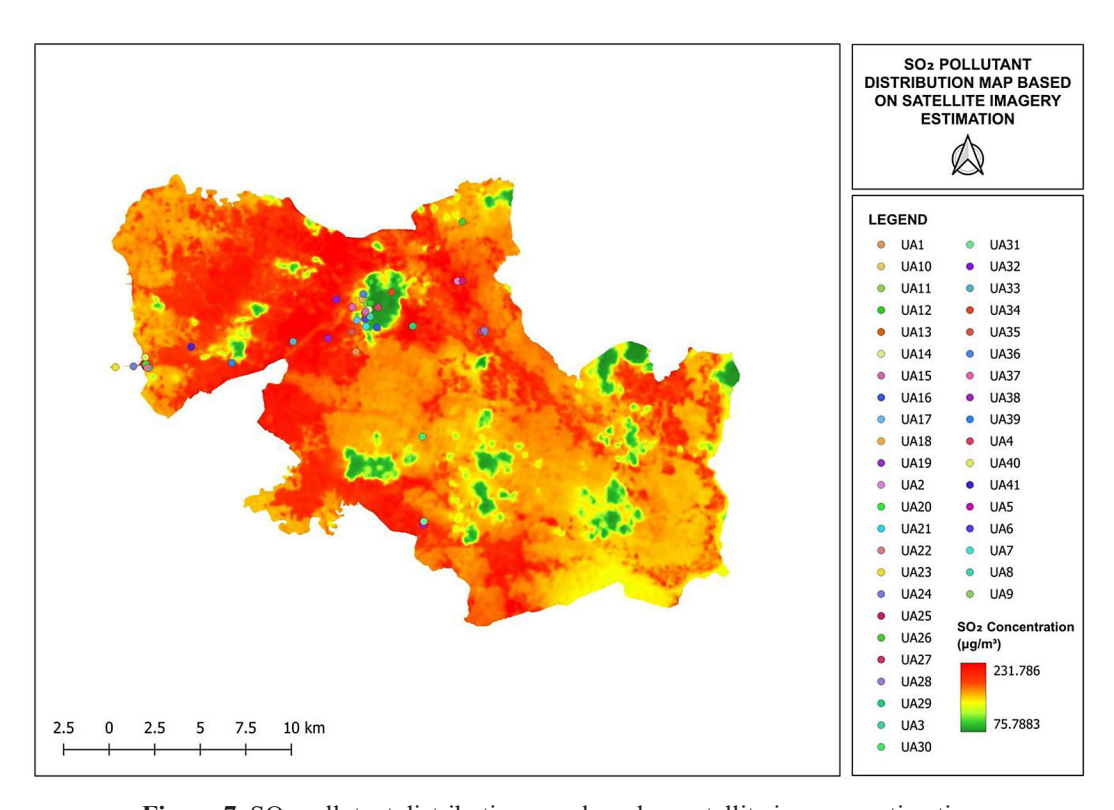


Figure 7. SO₂ pollutant distribution map based on satellite imagery estimation

assessment of environmental conditions. Table 3 presents the ISPU values derived from both ground-based measurements and satellite-based estimations.

Table 3 shows that while the ground-based ISPU values ranged from Good to Moderate, the satellite-derived ISPU values extended up to the Unhealthy category. These discrepancies highlight the impact of over- and underestimation in satellite-derived concentrations on the resulting index and emphasize both the potential as well as the limitations of remote sensing in representing actual air quality conditions.

DISCUSSION

The use of satellite imagery in estimating air pollutant concentrations is an innovative approach that enables spatial and temporal monitoring of air quality, particularly in the regions with limited conventional monitoring systems (Yan et al., 2025). In this study, the concentrations of four major air pollutants – PM₁₀, NO₂, SO₂, and CO – were estimated using the Landsat 8 data and empirical regression algorithms from previous research (Othman et al. (2010), Mahardianti et al. (2024), Somvanshi et al. (2019)).

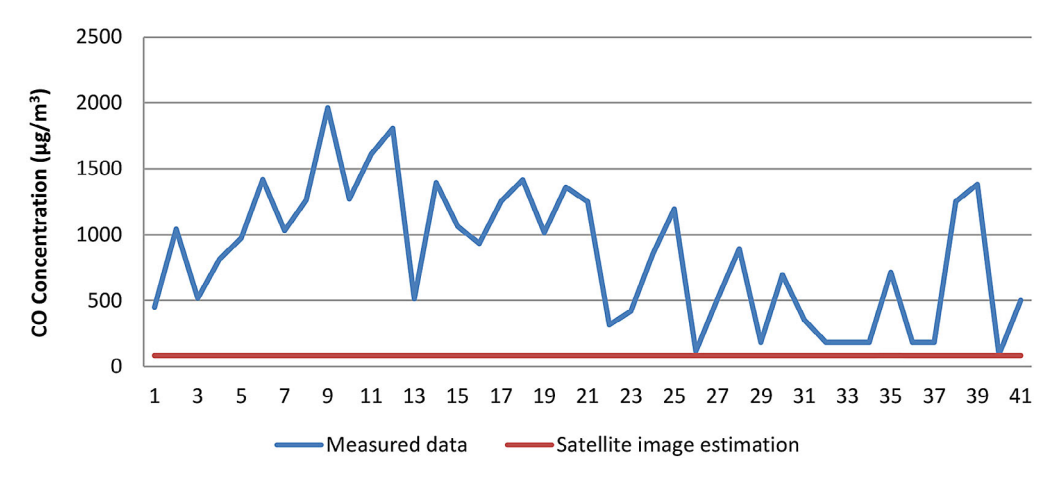


Figure 8. Comparison of the CO concentrations

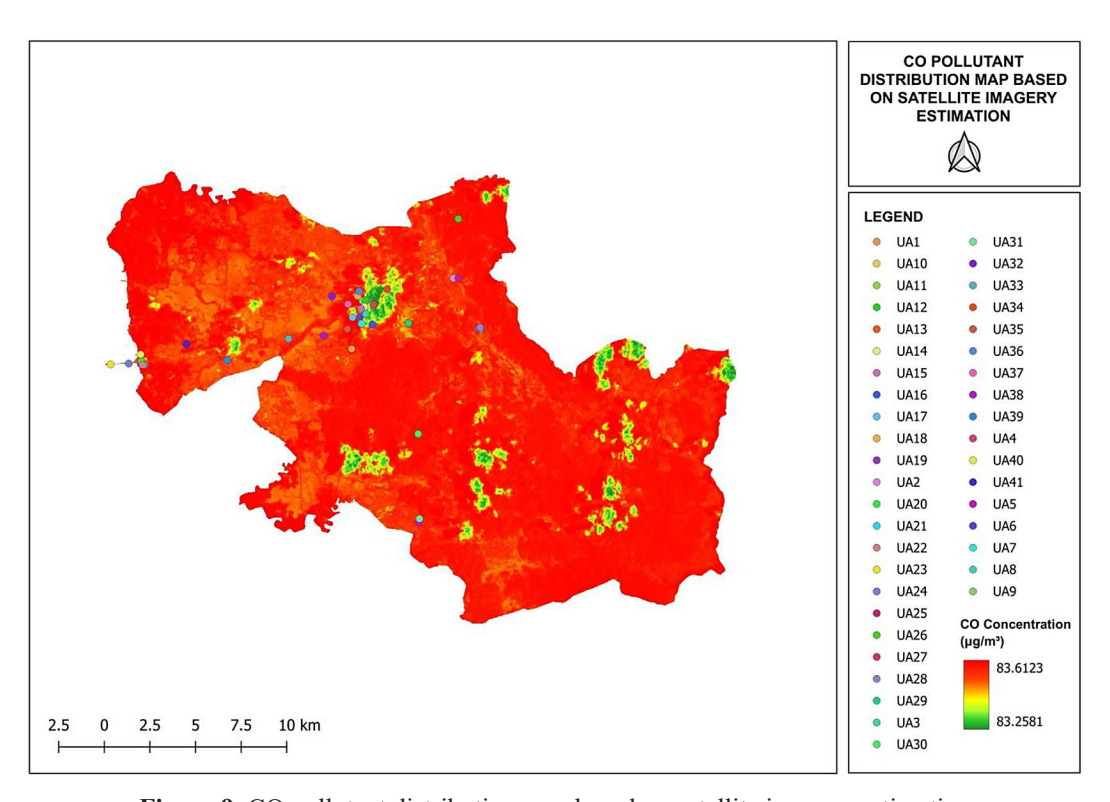


Figure 9. CO pollutant distribution map based on satellite imagery estimation

Particulate matter

On the basis of the distribution map derived from satellite image estimations (Figure 3), the highest PM₁₀ concentration was detected at point UA4 (Limestone Quarry). This can be attributed to open-pit mining and raw material transportation activities, which are known to be major sources of coarse particulate emissions in the cement industry (Al-Zboon et al., 2021). However, based on ground measurement data, the highest value was found at UA7 (Cement Mill Unit 5), indicating that cement grinding activities also serve as a major emission source due to intensive

mechanical processes (Elawa and Farahat, 2022). The difference in the highest concentration points between the satellite-based estimations and ground data highlights the limitations of satellite imagery in capturing highly localized emissions or those originating from enclosed sources. Nevertheless, the overall estimated distribution pattern is generally able to represent areas with high industrial activity intensity.

Nitrogen dioxide

For the NO₂ parameter, the estimation results indicated the highest concentration at UA2

Table 3. Air pollution standard index based on ground-based measurements and satellite imagery estimation

Area Me		Code		ISPU value		ISPU categories	
	Measurement points		Pollutant	Ground-based measurements	Satellite imagery estimation	Ground-based measurements	Satellite imagery estimation
			PM ₁₀	24.90	4.55	Good	Good
	Bontoa Clay	UA1	NO ₂	15.35	25.25	Good	Good
	Quarry	UAT	SO ₂	18.27	116.59	Good	Unhealthy
			CO	4.51	0.84	Good	Good
			PM ₁₀	25.60	4.55	Good	Good
	Tabo-Tabo Clay	1140	NO ₂	16.02	31.93	Good	Good
	Quarry	UA2	SO,	20.87	140.00	Good	Unhealthy
			CO	10.43	0.84	Good	Good
			PM ₁₀	31.50	4.55	Good	Good
	Bulutellue Clay	1140	NO,	18.50	29.13	Good	Good
	Quarry	UA3	SO,	24.33	130.20	Good	Unhealthy
			CO	5.18	0.84	Good	Good
			PM ₁₀	37.10	4.56	Good	Good
			NO ₂	21.99	10.44	Good	Good
	Limestone Quarry	UA4	SO ₂	27.21	62.51	Good	Moderate
			CO	8.15	0.83	Good	Good
			PM ₁₀	28.50	4.55	Good	Good
	Tonasa 1 Clay		NO ₂	18.54	59.59	Good	Good
	Quarry	UA5	SO ₂	26.83	131.81	Good	Unhealthy
			CO	9.73	0.84	Good	Good
	Packer Unit 5	UA6	PM ₁₀	40.19	4.55	Good	Good
			NO ₂	20.80	16.59	Good	Good
			SO ₂	40.19	85.08	Good	Moderate
			CO	14.18	0.83	Good	Good
	Cement Mill Unit 5	UA7	PM ₁₀	51.00	4.55	Moderate	Good
			NO ₂	15.93	17.62	Good	Good
			SO ₂	28.46	88.85	Good	Moderate
O			CO	10.31	0.83	Good	Good
Operational area	Kiln Unit 5	UA8	+	32.80	4.55	Good	Good
arca			PM ₁₀	19.42	11.45	Good	Good
			NO ₂	23.17	66.22	Good	Moderate
			SO ₂			Good	Good
				12.63 42.90	0.83 4.55	Good	
			PM ₁₀				Good
	Packer Unit 2/3/4		NO ₂	18.45	10.56	Good	Good
			SO ₂	30.77	62.97	Good	Moderate
			CO	19.63	0.83	Good	Good
		UA10	PM ₁₀	34.10	4.55	Good	Good
	Cement Mill Unit		NO ₂	18.05	14.20	Good	Good
	2/3		SO ₂	30.67	76.30	Good	Moderate
			CO	19.71	0.83	Good	Good
		UA11	PM ₁₀	34.42	4.55	Good	Good
	Coal Mill Unit 2/3		NO ₂	17.48	17.08	Good	Good
			SO ₂	34.42	86.87	Good	Moderate
			CO	16.11	0.84	Good	Good
			PM ₁₀	36.70	4.55	Good	Good
	Kiln Unit 2/3	UA12	NO ₂	20.22	11.26	Good	Good
	KIIII UIIIL 2/3	UAIZ	SO ₂	34.52	65.54	Good	Moderate
			CO	18.06	0.83	Good	Good
	Coal Stock Pile	UA13	PM ₁₀	46.70	4.55	Good	Good
			NO ₂	19.96	16.84	Good	Good
	Unit 2/3/4		SO ₂	20.87	86.00	Good	Moderate
			CO	5.14	0.84	Good	Good
			PM ₁₀	49.70	4.55	Good	Good
	Kilo I loit 4	UA14	NO ₂	21.50	18.76	Good	Good
	Kiln Unit 4		SO ₂	26.15	93.02	Good	Moderate
			CO	13.95	0.83	Good	Good

Cont. Table 3.

	Measurement points	Code	Pollutant	ISPU value		ISPU categories	
Area				Ground-based measurements	Satellite imagery estimation	Ground-based measurements	Satellite imagery estimation
			PM ₁₀	45.70	4.55	Good	Good
	Cement Mill Unit 4	UA15	NO ₂	20.75	17.79	Good	Good
	Comone will only	07110	SO ₂	32.50	89.47	Good	Moderate
			CO	10.62	0.84	Good	Good
			PM ₁₀	25.80	4.55	Good	Good
	Coal Stockpile	UA16	NO ₂	15.35	16.17	Good	Good
	Unit 5	0/110	SO ₂	20.87	0.84	Good	Moderate
			CO	9.32	83.52	Good	Good
			PM ₁₀	33.40	4.55	Good	Good
	Coal Stockpile	UA17	NO ₂	9.34	14.64	Good	Good
	Bontoa		SO ₂	22.60	77.92	Good	Moderate
			CO	12.54	0.84	Good	Good
			PM ₁₀	42.80	4.55	Good	Good
	Batching Plant	UA18	NO ₂	23.01	18.90	Good	Good
	Biringere		SO ₂	32.40	93.56	Good	Moderate
			CO	14.16	0.84	Good	Good
			PM ₁₀	36.10	4.55	Good	Good
	Biringkassi Coal	UA19	NO ₂	17.30	27.42	Good	Good
0 " 1	Warehouse		SO ₂	30.58	124.22	Good	Unhealthy
Operational area			CO	10.17	0.84	Good	Good
aica	Biringkassi Cement Silo	UA20	PM ₁₀	50.95	4.55	Moderate	Good
			NO ₂	18.23	28.01	Good	Good
			SO ₂	34.33	126.30	Good	Unhealthy
			CO	13.62	0.84	Good	Good
	Biringkassi Power Plant 1	UA21	PM ₁₀	35.67	4.55	Good	Good
			NO ₂	26.46	26.40	Good	Good
			SO ₂	35.67	120.62	Good	Unhealthy
			CO	12.49	0.84	Good	Good
		UA22	PM ₁₀	36.90	4.55	Good	Good
	Biringkassi Power Plant 2		NO ₂	16.95	26.65	Good	Good
			SO ₂	20.87	121.49	Good	Unhealthy
	Central Special Wharf of Biringkassi Wharf II Biringkassi	UA23 UA24	CO	3.17	0.84	Good	Good
			PM ₁₀	31.90	4.55	Good	Good
			NO ₂	16.24	21.97	Good	Good
			SO ₂	19.62	105.11	Good	Unhealthy
			CO	4.19	0.84	Good	Good
			PM ₁₀	43.90	4.55	Good	Good
			NO ₂	11.55 29.90	22.92 108.45	Good Good	Good Unhealthy
			CO	8.52	0.84	Good	Good
Residential area	Road near Tabo-	UA25	PM ₁₀	33.85	4.55	Good	Good
				14.16	30.42	Good	Good
	Tabo Clay Quarry		NO ₂	33.85	134.72	Good	Unhealthy
	, , , , , , , , , , , , , , , , , , ,		CO CO	11.96	0.84	Good	Good
			+	24.81	4.55	Good	Good
	Residential Area		PM ₁₀ NO ₂	14.07	22.75	Good	Good
	near Tabo-Tabo	UA26	SO ₂	24.81	107.84	Good	Unhealthy
	Quarry		CO	1.15	0.84	Good	Good
		UA27	PM ₁₀	30.80	4.55	Good	Good
	Residential Area		NO ₂	19.07	28.44	Good	Good
	near Bulutellue		SO ₂	18.27	127.80	Good	Unhealthy
	Quarry		CO	5.16	0.84	Good	Good
			+	21.80	4.55	Good	Good
	Road near		PM ₁₀	17.48	28.53	Good	Good
	Bulutellue Clay	UA28 -	NO ₂	18.27	128.12	Good	Unhealthy
	Quarry		CO	8.94	0.84	Good	Good
				0.94	0.04	Good	G000

Cont. Table 3.

		Code	Pollutant	ISPU value		ISPU categories	
Area Measurement points	Measurement points			Ground-based measurements	Satellite imagery estimation	Ground-based measurements	Satellite imagery estimation
			PM ₁₀	24.10	4.55	Good	Good
	Mangilu Village	UA29	NO ₂	6.42	30.71	Good	Good
	Wangila Village	UAZS	SO ₂	18.27	135.74	Good	Unhealthy
			CO	1.84	0.84	Good	Good
			PM ₁₀	30.20	4.55	Good	Good
	Road near Tonasa	UA30	NO ₂	17.57	22.93	Good	Good
	1 Clay Quarry	UASU	SO ₂	26.54	108.49	Good	Unhealthy
			CO	6.95	0.84	Good	Good
	Decidential Asses		PM ₁₀	25.80	4.55	Good	Good
	Residential Area near Tonasa 1	UA31	NO ₂	18.23	29.35	Good	Good
	Clay Quarry	OAOT	SO ₂	18.27	130.97	Good	Unhealthy
			CO	3.53	0.84	Good	Good
			PM ₁₀	21.80	4.55	Good	Good
	Taraweang Village	UA32	NO ₂	7.83	30.76	Good	Good
	Tarawcang village	UAUZ	SO ₂	18.27	135.92	Good	Unhealthy
			СО	1.84	0.84	Good	Good
	In Front of Sapanang Village Office	UA33	PM ₁₀	25.30	4.55	Good	Good
			NO ₂	12.92	30.75	Good	Good
Residential area			SO ₂	18.27	135.87	Good	Unhealthy
			СО	1.84	0.84	Good	Good
	In Frank of	UA34	PM ₁₀	22.90	4.55	Good	Good
	In Front of Kampung Sela Mosque		NO ₂	16.90	13.21	Good	Good
			SO ₂	18.27	72.69	Good	Moderate
			СО	1.84	0.83	Good	Good
	In Front of Main Office	UA35	PM ₁₀	31.80	4.55	Good	Good
			NO ₂	18.45	26.15	Good	Good
			SO ₂	28.75	119.76	Good	Unhealthy
			CO	7.14	0.84	Good	Good
		UA36	PM ₁₀	31.50	4.55	Good	Good
	Biringere Village Office		NO ₂	10.18	20.35	Good	Good
			SO ₂	20.77	98.85	Good	Moderate
			СО	1.84	0.84	Good	Good
	In Front of Taqwa Mosque	UA37	PM ₁₀	23.60	4.55	Good	Good
			NO ₂	7.48	26.01	Good	Good
			SO ₂	18.27	119.30	Good	Unhealthy
			CO	1.84	0.84	Good	Good
	Tonasa–Bungoro Main Road (Bontoa)	UA38	PM ₁₀	37.20	4.55	Good	Good
			NO ₂	16.50	30.68	Good	Good
			SO ₂	49.33	135.63	Good	Unhealthy
			СО	12.52	0.84	Good	Good
		UA39	PM ₁₀	39.20	4.55	Good	Good
	Bungoro Intersection		NO ₂	20.44	28.58	Good	Good
			SO ₂	49.04	128.29	Good	Unhealthy
			СО	13.82	0.84	Good	Good
	In Front of	UA40	PM ₁₀	21.40	4.55	Good	Good
	Bujung Tangaya		NO ₂	11.19	26.87	Good	Good
	Elementary School (Bulu Cindea)		SO ₂	15.48	122.27	Good	Unhealthy
	(Duid Cilidea)		CO	0.90	0.84	Good	Good
			PM ₁₀	21.50	4.55	Good	Good
	Bowong Cindea	UA41	NO ₂	16.24	26.99	Good	Good
	Village		SO ₂	20.00	122.71	Good	Unhealthy
			CO	5.01	0.84	Good	Good

(Tabo-Tabo Clay Quarry), while ground measurements showed the highest value at UA21 (Biringkassi Power Plant 1) (Figures 4 and 5). The high NO₂ concentration in the power plant area is expected, as coal combustion is a major source of NO, emissions (Agarwalla et al., 2024). However, the high estimated concentration in the mining area suggests potential algorithmic bias toward open surfaces with high land surface temperatures, as LST (Land Surface Temperature) is a contributing variable in the estimation algorithm. Rahaman et al. (2023) have noted that the NO2 concentration estimates using the multiband approach from Landsat may deviate in areas with low vegetation cover or bright surfaces such as mining zones.

Sulfur dioxide

The estimated SO₂ distribution showed the highest concentration at UA2 (Tabo-Tabo Clay Quarry), while ground measurements identified the peak at UA38 (Tonasa-Bungoro Main Road (Bontoa)) (Figures 6 and 7). The SO₂ pollutants typically originate from the combustion of high-sulfur fuels, such as coal in power plants and industrial transportation (Etim et al., 2021). This discrepancy is likely influenced by the temporal resolution limitations of Landsat 8 imagery, which only captures data every 16 days, potentially causing the estimation to miss the actual conditions at the time of ground measurement. Nevertheless, the distribution pattern indicates that the estimation algorithm by Mahardianti et al. (2024) still effectively captures the general trend of SO₂ distribution, particularly in industrial areas with combustion and raw material processing activities.

Carbon monoxide

For the CO parameter, the estimation indicated the highest concentration at UA35 (In Front of Main Office), while measurement data recorded the peak at UA9 (Packer Unit 2/3/4) (Figures 8 and 9). Carbon monoxide is an invisible and scentless gas generated through incomplete combustion processes, mainly originating from motor vehicles and industrial equipment (World Health Organization, 2021). The estimation model applied was based on the approach by Somvanshi et al. (2019), which utilized a combination of OLI and TIRS bands, including land surface temperature as a parameter. Potential discrepancies may

arise because the CO levels fluctuate rapidly and are heavily influenced by daily human activities, which may not be captured during satellite acquisition times. Moreover, CO is a light gas that can be quickly diluted by wind, making its spatial distribution highly dynamic (Bachtiar et al., 2018).

The comparison between estimation results and measurement data indicates that satellite imagery-based approaches hold strong potential for mapping regional air pollution. However, discrepancies exist between the locations of the highest estimated concentrations and those of the actual measured peaks across nearly all parameters. This aligns with the findings of Ghasempour et al. (2021), who noted that the accuracy of satellite-based estimations is highly dependent on atmospheric conditions, surface characteristics, and the timing of image acquisition.

Several factors influence the accuracy of satellite-derived air pollutant concentration estimates. First, spatial resolution limitations—such as the 30-meter resolution of Landsat 8-make it less effective in precisely detecting point-source emissions, particularly from localized sources such as factory chimneys or heavy vehicles. Second, the estimation algorithms rely heavily on land surface temperature (LST) and vegetation indices. This dependence can lead to inaccuracies, especially in artificial or open mining areas the surface characteristics of which differ significantly from vegetated regions. Third, temporal variability of emissions poses a challenge, as air pollutant concentrations are strongly influenced by daily human activities and rapidly changing meteorological conditions. Since satellite imagery captures only a single moment in time, it may not align with the timing of ground measurements (Shin et al., 2020).

Nevertheless, this approach remains highly valuable, especially in the areas with limited air quality monitoring infrastructure. As reported by IQAir (2024), South Sulawesi has only three air monitoring stations, making the application of remote sensing technology a relevant and efficient alternative solution.

Furthermore, air pollutant concentrations estimated from satellite imagery were used to calculate the Indonesian Air Pollution Standard Index (ISPU) based on Government Regulation No. 22 of 2021. The estimation results at 41 measurement points revealed a wide range of air quality categories. According to the ISPU, several locations fell under the Unhealthy category,

particularly in industrial areas such as Tabo-Tabo Clay Quarry (UA2), Biringkassi Cement Silo (UA20), and residential zones near major emission sources. These findings signal possible pollutant exposure that may adversely affect public health, particularly among sensitive populations such as children and the elderly.

However, when ISPU values were calculated using direct measurement data (on-site test results), the outcomes differed significantly. All points were recorded in the Good category, with some ranging up to Moderate. These discrepancies indicate a potential overestimation in the satellite-based results. This may occur because some estimation algorithms assume ideal conditions in the relationship between spectral values and pollutant concentrations, whereas local atmospheric conditions, surface disturbances, and the timing of image acquisition greatly affect estimation accuracy. As Wang et al. (2022) noted, factors such as humidity, land surface temperature, and the presence of aerosols can influence the accuracy of remote sensing-based calculations.

Therefore, while satellite-based approaches offer advantages in terms of broad and continuous monitoring, their results must be regularly validated against ground-based measurements to achieve a more accurate understanding of air quality. These inconsistencies also highlight the need to develop localized algorithms that are better suited to the atmospheric and land use characteristics of the study area, as well as the importance of selecting acquisition times that better reflect daily pollution conditions on the ground. A combined approach using satellite imagery and direct measurements can provide more reliable results to support air pollution control policies, particularly in strategic industrial areas such as Pangkep Regency.

Several previous studies have demonstrated the potential of satellite remote sensing for assessing air quality in diverse environments, including arid regions, urban megacities, and industrial areas (Othman et al., 2010; Mahardianti et al., 2024; Somvanshi et al., 2019). These studies indicate that satellite-derived data can be used to estimate air quality parameters and indices, although discrepancies with ground-based measurements remain a common challenge.

At the same time, this study provides the contributions that distinguish it from much of the earlier work. While previous research has focused on arid regions, large urban centers, or

industrial—urban areas, the present study examines a cement industrial complex characterized by highly localized and intense emissions. This industrial context highlights both the strengths and the limitations of medium-resolution satellite imagery in representing pollutant variability across heterogeneous landscapes. Furthermore, the integration of satellite-derived pollutant concentrations with ISPU provides a framework that has rarely been emphasized in earlier studies, particularly in the context of Indonesia.

These aspects underline the significance of this research. By combining satellite-based estimations with ground-based measurements, the study demonstrates a practical approach for assessing air quality in the regions where monitoring infrastructure is limited. The results suggest that, despite a tendency to overestimate concentrations, satellite remote sensing can serve as a valuable complementary tool for identifying pollution hotspots and providing broader spatial coverage. This integrated approach not only supports environmental monitoring and management in industrial regions but also contributes to policymaking aimed at balancing industrial development with public health protection.

CONCLUSIONS

This study demonstrated the potential of Landsat 8 imagery for estimating concentrations of PM₁₀, NO₂, SO₂, and CO in an industrial cement area of Pangkep Regency, South Sulawesi, with validation against ground-based data. The results showed that the NO, and SO, concentrations were generally overestimated by satellite estimations, while PM₁₀ and CO were underestimated compared with field observations, leading to notable differences in ISPU values. The ground-based ISPU ranged from Good to Moderate, whereas the satellite-derived ISPU extended to categories as high as Unhealthy, reflecting the influence of resolution, surface heterogeneity, and acquisition timing on pollutant estimation. Despite these discrepancies, the integration of the satellite and ground-based approaches highlights the usefulness of remote sensing for identifying spatial variability and potential pollution hotspots, especially in the areas with limited monitoring infrastructure. These findings emphasize the role of satellite data as a complementary tool for environmental management

and policy-making in industrial regions, while also pointing to the need for future research that incorporates higher-resolution sensors, multitemporal datasets, and advanced modeling techniques to improve accuracy and reliability in satellite-based air quality assessments.

REFERENCES

- Agarwalla, H., Gangopadhyay, M., Masto, R., Bari, S., Kumar, M. (2024). Environmental Emission from Coal-Fired Power Plant and Control Technology 163–171. https://doi. org/10.1007/978-981-97-1363-9 12
- 2. Al-Zboon, K., Matalqah, W., Ammary, B. (2021). Effect of cement industry on ambient air quality and potential health risk: A case study from Riyadh, Saudi Arabia. *Jordanian Journal of Engineering & Chemical Industries*, 4(1).
- 3. Almetwally, A. A., Bin-Jumah, M., Allam, A. A. (2020). Ambient air pollution and its influence on human health and welfare: an overview. *Environmental Science and Pollution Research*, 27, 24815–24830.
- Bachtiar, V. S., Purnawan, P., Afrianita, R., Dahlia, N. (2018). Effect of Wind Angle Direction on Carbon Monoxide (CO) Concentration Dispersion on Traffic Flow in Padang City. *IOP Conference Series: Materials Science and Engineering*, 288(1), 12146. https://doi.org/10.1088/1757-899X/288/1/012146
- Brontowiyono, W., Sihayuardhi, E. R., Maziya, F. B., Hakim, L. (2022). Distribution patterns of ambient air quality pre- and during pandemic in the urban area of Yogyakarta, Indonesia. *Journal of Ecological Engineering*, 23(10), 116–128. https://doi.org/10.12911/22998993/152362
- Chen, F., Zhang, W., Mfarrej, M. F. B., Saleem, M. H., Khan, K. A., Ma, J., Raposo, A., Han, H. (2024). Breathing in danger: Understanding the multifaceted impact of air pollution on health impacts. *Ecotoxicology and Environmental Safety*, 280, 116532. https://doi.org/https://doi.org/10.1016/j.ecoenv.2024.116532
- Drahman, S. H., Maseri, H., Nap, M. C., Hossen, Z. B. (2024). Twenty Years of air pollutant index trend analysis in Kuching, Sarawak, Malaysia (2000-2019). Sains Malaysiana, 53(3), 623–633.
- 8. Elawa, O. I., Farahat, E. A. (2022). Assessment of ambient air quality level at 21 sites in cement sector, Egypt. *Egyptian Journal of Chemistry*, 65(9), 47–57.
- Etim, M.-A., Babaremu, K., Lazarus, J., Omole, D. (2021). Health risk and environmental assessment of cement production in Nigeria. *Atmosphere*, 12(9), 1111.

- Ghasempour, F., Sekertekin, A., Kutoglu, S. H. (2021). Google Earth Engine based spatio-temporal analysis of air pollutants before and during the first wave COVID-19 outbreak over Turkey via remote sensing. *Journal of Cleaner Production*, 319, 128599.
- IQAir. (2024). Kualitas Udara di Sulawesi Selatan. https://www.iqair.com/id/indonesia/southsulawesi?srsltid=AfmBOor3osaO-M4QrhQ7s1K-Dxi9obqDf3zy9NBO9PWMyh4hVgiGQa0bM
- 12. Jasiński, R. (2024). Analysis of the applied flight trajectory influence on the air pollution in the area of Warsaw Chopin Airport. *Journal of Ecological Engineering*, 25(5), 294–305. https://doi.org/10.12911/22998993/186440
- 13. John, G., Semenova, E. A., Mohamed, D. A., Georges Abi Antoun, T., Yusupov, R. A., Ahmetov, I. I. (2025). Air pollution and its impact on health and performance in football players. In *Sports 13*(6). https://doi.org/10.3390/sports13060170
- 14. Kuntic, M., Kuntic, I., Hahad, O., Lelieveld, J., Münzel, T., Daiber, A. (2023). Impact of air pollution on cardiovascular aging. *Mechanisms of Ageing and Development*, 111857.
- 15. Mahardianti, M. A., Prabawa, S. E., Effendi, A. F. (2024). Studi perubahan indeks kerapatan vegetasi terhadap suhu permukaan tanah dan indeks kualitas udara dengan pemanfaatan citra satelit Landsat 8 di kabupaten Gresik. GEOID, 19(3), 386–404.
- 16. Mohammed, A., Bakar, M. A. A. B. U., Mansor, M. M., Ariff, N. M. (2024). Modelling Malaysia air quality data using bayesian structural time series models (memodelkan data kualiti udara Malaysia menggunakan model siri masa berstruktur bayesian). Sains Malaysiana, 53(11), 3817–3829.
- 17. Nakhjiri, A., Kakroodi, A. A. (2024). Air pollution in industrial clusters: A comprehensive analysis and prediction using multi-source data. *Ecological Informatics*, 80, 102504. https://doi.org/10.1016/j.ecoinf.2024.102504
- 18. NASA. (2024). *Landsat-8*. https://landsat.gsfc.nasa.gov/satellites/landsat-8/
- 19. Othman, N., Jafri, M. Z. M., San, L. H. (2010). Estimating particulate matter concentration over arid region using satellite remote sensing: A case study in Makkah, Saudi Arabia. *Modern Applied Science*, *4*(11), 131.
- 20. Pambudi, R. A., Naldi, A., Luthfi, A., Puspitarini, D. A., Chaerani, M. M., Permana, M. W., Shafira, S. (2020). Spatiotemporal trend of particulate matter (PM10) concentration on cement industries in Klapanunggal and Citeureup Sub-districts. *IOP Conference Series: Earth and Environmental Science*, 561(1), 12035.
- 21. Rahaman, S. N., Ahmed, S. M. M., Zeyad, M., Zim, A. (2023). Effect of vegetation and land surface temperature on NO₂ concentration: A Google

- Earth Engine-based remote sensing approach. *Urban Climate*, 47, 101336. https://doi.org/10.1016/j.uclim.2022.101336
- 22. Sannigrahi, S., Kumar, P., Molter, A., Zhang, Q., Basu, B., Basu, A. S., Pilla, F. (2021). Examining the status of improved air quality in world cities due to COVID-19 led temporary reduction in anthropogenic emissions. *Environmental Research*, 196, 110927.
- 23. Shin, M., Yoojin, K., Seohui, P., Jungho, I., Cheolhee, Y., Quackenbush, L. J. (2020). Estimating ground-level particulate matter concentrations using satellite-based data: a review. GIScience & Remote Sensing, 57(2), 174–189. https://doi.org/10.1080/15481603.2019.1703288
- 24. Siddiqua, A., Hahladakis, J. N., Al-Attiya, W. A. K. A. (2022). An overview of the environmental pollution and health effects associated with waste landfilling and open dumping. *Environmental Science and Pollution Research*, 29(39), 58514–58536.
- 25. Singh, A., Singh, K. K. (2022). An overview of the environmental and health consequences of air pollution. *Iranica Journal of Energy & Environment*, 13(3), 231–237.
- 26. Somvanshi, S. S., Vashisht, A., Chandra, U., Kaushik, G. (2019). Delhi air pollution modeling using remote sensing technique. *Handbook of Environmental Materials Management*, 1–27.
- 27. South Australia EPA. (2023). *Importance of Clean Air*. https://soe.epa.sa.gov.au/environmental-themes/air/importance-of-clean-air#:~:text=Clean air is essential for impacting soil quality and waterbodies.

- 28. Taufieq, N. A. S., Pertiwi, N., Salsabila, P. H., Firmansyah, M. (2024). Estimated CO and NO 2 emissions due to conventional brick kilns in Sidrap Regency, South Sulawesi, Indonesia. *International Journal on Advanced Science, Engineering & In*formation Technology, 14(4).
- 29. Thongtip, S., Srivichai, P., Chaitiang, N., Tantra-karnapa, K. (2022). The influence of air pollution on disease and related health problems in northern Thailand. *Sains Malaysiana*, *51*(7), 1993–2002.
- 30. United Nations. (2024). *International Day of Clean Air for Blue Skies*. https://www.un.org/en/observances/clean-air-day
- 31. Venkata Sudhakar, C., Reddy, U. (2023). Impacts of cement industry air pollutants on the environment and satellite data applications for air quality monitoring and management. *Environ Monit Assess*, 195(840), 840.
- 32. Wang, Y., Cai, G., Yang, L., Zhang, N., Du, M. (2022). Monitoring of urban ecological environment including air quality using satellite imagery. *Plos One*, *17*(8), e0266759.
- 33. World Health Organization. (2021). Air quality, energy and health. https://www.who.int/teams/environment-climate-change-and-health/air-quality-and-health/health-impacts/types-of-pollutants
- 34. Yan, X., Wang, J., Wu, F., Bai, J., Zhang, X., Li, G., Fei, H. (2025). Spatial and temporal variation characteristics of air pollutants in coastal areas of China: From satellite perspective. In *Remote Sensing 17*(11). https://doi.org/10.3390/rs17111861